Processing and Application of Ceramics 19 [2] (2025) 121–127
https://doi.org/10.2298/

Effect of Ni content on mechanical properties and corrosion resistance of WC-Co-Ni cemented carbides

Shubo Xu*, Hui Xue, Hailong Ma, Siyu Sun, Yuefei Pan, Jianing Li, Guocheng Ren

Shandong Jianzhu University, School of Materials Science and Engineering, Jinan, 250101, China

Received 18 November 2024; Received in revised form 14 May 2025; Accepted 19 May 2025

Abstract

WC-Co-Ni cemented carbides with 90 wt.% WC and different Co/Ni ratios (WC-(1−x)Co-xNi, where x = 0, 1, 3, 5, 7 and 9 wt.%) were prepared by powder metallurgy method. The aim was to study the microstructure of these carbides, analyse their mechanical properties and investigate their corrosion resistance and thus find the optimal Co/Ni ratio for the fabrication of reliable cutting tools. The results show that with the increase of Ni content, the grain size and inhomogeneity gradually increase. On the other hand, the hardness, wear resistance and flexural strength of WC-Co-Ni cemented carbides decrease. The fracture toughness firstly increases and then decreases while the corrosion resistance is enhanced. The WC-7Co-3Ni specimen had the best comprehensive mechanical properties compared to other composites. This, together with the improved corrosion and damage resistance, confirmed that the WC-7Co-3Ni composite could substantially extend the working life of shield machine tools.

Keywords: *WC-Co-Ni cemented carbides, microstructure, mechanical properties, corrosion resistance*

I. Introduction

The invention of the subway has had a profound impact on city life. It not only greatly relieves the pressure of ground transportation, but also improves people's travel efficiency [1]. To promote the close connection between urban areas, subway construction often needs to cross busy metropolitan areas and complex geological conditions, which requires the construction process to be characterized by high efficiency, safety and environmental protection [2,3]. Shield machines, as special engineering machinery for tunnelling, have become indispensable equipment for subway construction due to their advantages of high automation [4–6], labour-saving, fast construction speed, one-time hole formation [7–9] and ground settlement control during excavation. Metro shield machines can excavate the soil while advancing along the tunnel axis, and at the same time protect the excavated tunnel section and withstand the pressure of the surrounding soil layer to ensure the safety and stability of the construction process. Different types of shield machines can also be adapted to different geological conditions, providing more choices and flexibility for subway construction [10,11]. The working principle of the shield machine's cutter head is mainly to cut rocks and soil into small pieces by rotating the blades in the cutter head and discharging them out of the tunnel [12]. The design of the blade and the choice of material have an important impact on the cutting ability and life of the cutter head, so it is particularly important to develop shield machine cutting tools with good toughness and corrosion resistance [13–15].

Traditional WC-Co cemented carbides have relatively limited toughness and may fracture or break when subjected to strong impacts or vibrations, [16,17], especially in harsh and unstable working environments where this risk is higher. Cobalt content is one of the key factors affecting the performance of WC-Co cemented carbides [18–20]. Too high or too low Co content will lead to the decrease in the performance of the samples. Therefore, the content of cobalt needs to be strictly controlled during the preparation process to ensure that the specimen has the best performance. Co is a scarce metal with extremely limited world reserves, which leads to the increasing price of Co, so it is essential to seek a material that can replace Co. The potential candidate is nickel. Ni and Co belong to the transition group of metals [21], have similar physical and chemical prop-

* Corresponding authors: tel: +86 15153166968,
e-mail: *xsb@sdjzu.edu.cn*

erties, but production and reserves of Ni are far more greater than that of Co [22–24]. In addition, nickel antioxidant behaviour is much better than that of Co that can be used to make up for the shortcomings of the pure Co bonding phase which is easily corroded. Therefore, Ni can meet the basic requirements as a binder phase in cemented carbides having application in a severe environment [22,25].

To prove the feasibility of Ni replacing part of Co as the binder phase, in this paper six groups of WC-Co-Ni cemented carbide specimens with different Ni and Co contents (in all samples, the mass fraction of WC is consistently 90 wt.%) were prepared to find an optimal cobalt-nickel ratio by testing their mechanical properties, microstructure and corrosion resistance. To simulate the working environment of shield machine tools, the polarization curve analysis was performed in 3.5% NaCl electrolyte solution and the corrosion resistance of the prepared WC-Co-Ni cemented carbides with different Ni-content was also investigated.

II. Experimental

2.1. Materials and methods

WC-Co-Ni samples with different Co/Ni ratios (Table 1) were prepared by using powder metallurgy method (Fig. 1). The used raw materials were: WC powder (Jinan Metallurgical Science Research Institute Co. Ltd), Co powder ((Jinan Metallurgical Science Research Institute Co. Ltd) and Ni powder (Jinan Metallurgical Science Research Institute Co. Ltd), with their parameters listed in Table 2.

Six groups of powder mixtures were poured into ball milling jars with a ball-to-powder ratio of 2:1. Using 23% alcohol as the dispersing medium, the mixtures were wet-milled for 16 h in a GQM-4-5 roller ball mill at a speed of 60 rpm. The wet-milled mixtures were then dried in a vacuum drying oven. After that 2% paraffin wax dissolved in gasoline was added to the mixed powders and the obtained samples were pressed using a 30T single-column hydraulic press under a pressure of 15 kN. The resulting pellets were sintered in a PVA low-pressure sintering furnace at 1450 °C under an argon atmosphere. After sintering, the samples were ground to the required dimensions using a grinding machine, as shown in Fig. 2. The surface oxide layer was removed and polished using a polishing machine. The samples were sequentially polished with 6, 3 and 1 μm polishing solutions to achieve a surface roughness below 1 μm. Subsequently, these samples were subjected to mechanical property and corrosion resistance tests.

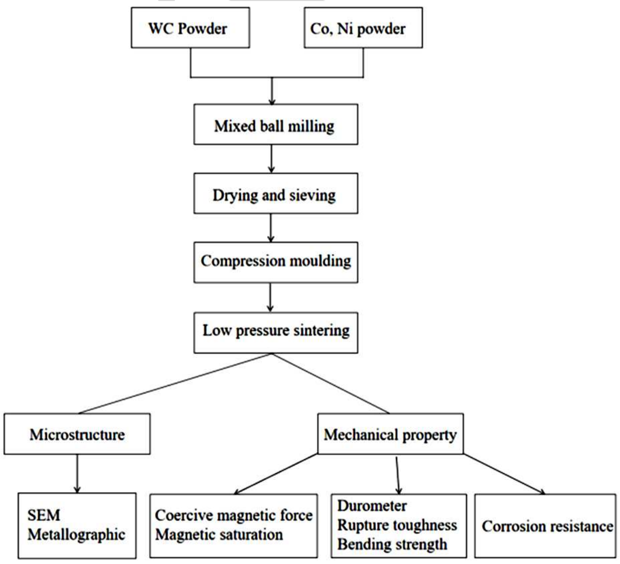

Figure 1. Experimental flow

Table 1. Composition ratio of ceramic specimens

Specimen	ω_{WC} [wt.%]	ω_{Co}:ω_{Ni}
WC-10Co	90	-
WC-9Co-1Ni	90	9:1
WC-7Co-3Ni	90	7:3
WC-5Co-5Ni	90	5:5
WC-3Co-7Ni	90	3:7
WC-1Co-9Ni	90	1:9

Table 2. Characteristics of raw powders

Powder	Fichte's particle size [μm]	Major chemical composition
WC	1.1–1.4	Total carbon: 6.13 ± 0.05%; free carbon: 0.06%; O: 0.12%
Co	1–2	Co ≥ 98.0%; Fe: 0.3%; C: 0.1%; O: 0.5%
Ni	2.5	Ni ≥ 99.8%; O: 0.15%; Fe: 0.006%

Figure 2. Shape of ceramic specimen after sintering

2.2. Characterization

The fracture toughness of the samples was tested using a PWS-100/V3.0 universal testing machine. The bending strength of the samples was measured using a WDW-100L microcomputer-controlled electronic universal testing machine. The Rockwell hardness of the samples was determined using a German WH2002T hardness tester, and the Vickers hardness was measured using an MHVD-50AP multifunctional turret digital display Vickers hardness tester. The microstructure of the samples was observed using a Leica DMI3000M

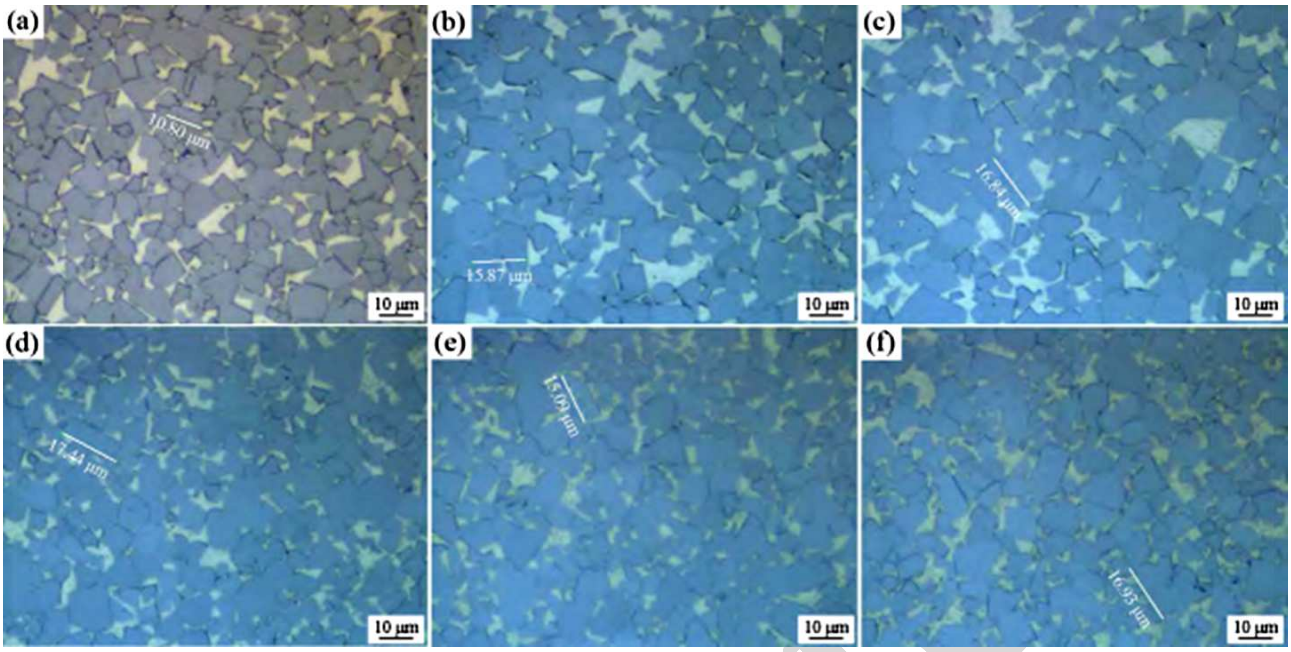

Figure 3. Metallographic micrographs of specimens with different compositions: a) WC-10Co, b) WC-9Co-1Ni, c) WC-7Co-3Ni, d) WC-5Co-5Ni, e) WC-3Co-7Ni and f) WC-1Co-9Ni

metallographic microscope. The surface morphology was examined using a scanning electron microscope (SEM, PW-100-018) and the chemical composition of the sample surface was analysed using the energy-dispersive spectroscopy (EDS) system integrated with the SEM.

Electrochemical experiments were conducted using a three-electrode system, where the composite sample served as the working electrode, a saturated calomel electrode (SCE) as the reference electrode, and a platinum electrode as the counter electrode. The electrochemical workstation used was a CHI604E model. The cemented carbide samples, after cleaning, were sealed with wax, exposing a surface area of 6.5 mm × 5.25 mm as the working surface and left to solidify at room temperature for 0.5 h. The corrosion solution with 3.5% NaCl was used to simulate spring water solution with pH of 7. The scanning potential range was set based on the open-circuit potential of each sample ±200 mV, and the scanning rate was set at 1 mV/s. For each performance test, 5 to 8 samples were required (3 to 5 samples were sufficient for wear resistance testing) to reduce experimental errors and ensure the accuracy and stability of the test results.

III. Results and discussion

3.1. Microstructure analysis

By comparing the metallographic micrographs of the samples with different Ni content, it can be seen (Fig. 3) that the WC-Co-Ni cemented carbide grains with uniform sizes are homogeneously distributed in Co and Ni bonding phases. There are no large areas of bonding phases as well as no carburization and decarburization phenomena. This indicates that Ni addition does not have a great influence on the structural uniformity.

A binder phase can inhibit the growth of WC grains. Thus, with the increase of the binder phase content the distribution of grains at the boundaries becomes more uniform, hindering the diffusion and growth of WC grains, thereby leading to the reduction in grain size. The addition of Ni may alter the sintering kinetics of WC-Co-Ni cemented carbides, reducing the mobility of grain boundaries and thus achieving the purpose of grain refinement. In the prepared samples, only the Co/Ni mass ratio was adjusted, and the change in grain size of the cemented carbides was not significant, as the inhibitory effects of Ni and Co on grain growth were similar.

Figure 4 shows SEM images of the WC-Co-Ni cemented carbides with different Ni contents. As it can be seen, the distribution of WC in the binder phase in the WC-10Co specimen is very uniform, but with the increasing Ni content, the WC grain size increases subsequently and the uniformity of WC grain size distribution decreases. For the samples with 5, 7 and 9 wt.% Ni the grain inhomogeneity becomes more and more obvious and the degree of grain inhomogeneity reaches the maximum in the WC-1Co-9Ni composite. There are large areas of bonding phase in the WC-1Co-9Ni sample. The reason could be the higher solubility of WC in the bonding phase containing Ni than that with Co, since the solubility range in Ni is generally 12% to 20%, and in Co it is 10% to 15%. When the carbon content and the total amount of binder phase in the sample are the same, the amount of the liquid phase at the same sintering temperature in the composite containing Ni is higher compared to the WC-Co ceramics. Thus, with the increase of Ni content the dissolution-precipitation rate of WC grains rises and the use of Ni to partially or completely replace

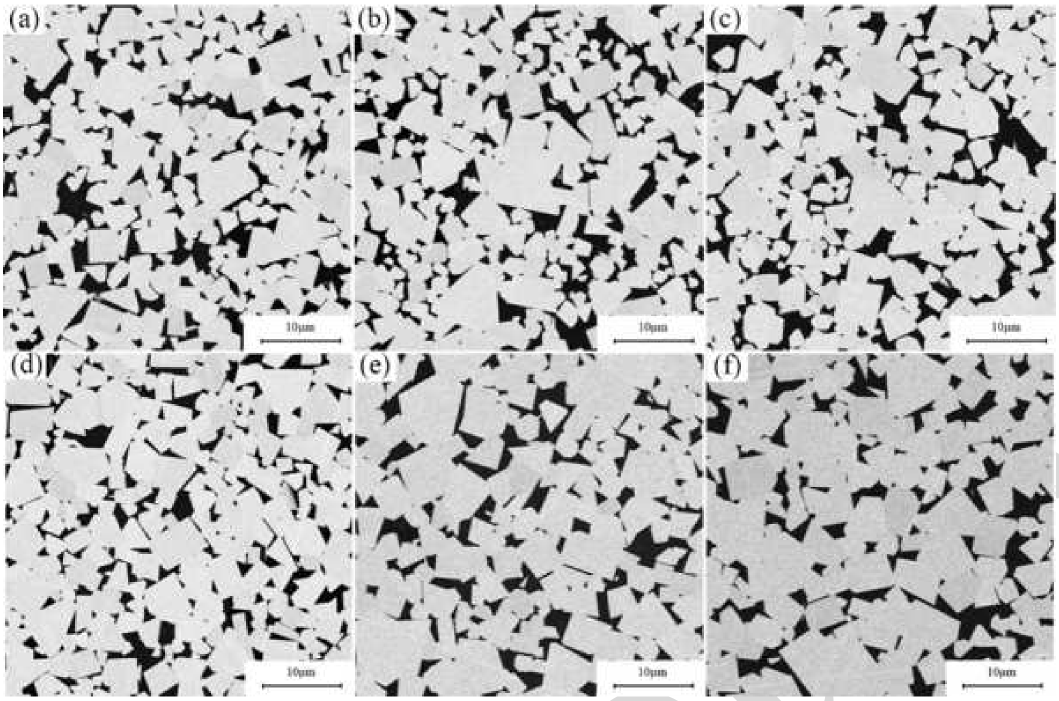

Figure 4. SEM images of specimens with different compositions: a) WC-10Co, b) WC-9Co-1Ni, c) WC-7Co-3Ni, d) WC-5Co-5Ni, e) WC-3Co-7Ni and f) WC-1Co-9Ni

Co leads to the cemented carbide with larger amount of bonded phase and less uniform WC grain size distribution.

3.2. Density and hardness

The Archimedes' water displacement method was used to measure the sample density. Since the densities of Ni and Co are much lower than that of WC, the overall density of the composite is lower than that for the pure WC. However, when the total content of Ni and Co remains unchanged and only the Co/Ni ratio is adjusted, the density of the WC-Co-Ni composites has minimal variation, generally around 14.45 g/cm^3.

Figure 5 shows the hardness of the cemented carbides with different Co to Ni ratios. It can be seen that the hardness of the cemented carbide specimen decreases with the increase of Ni content. This is because the hardness of cemented carbides is mainly related to the WC grain size according to the Hall-Petch equation:

$$H_v = 550 + \frac{23.5}{\sqrt{d_{\text{WC}}}} \tag{1}$$

where H_v is Vickers hardness and d_{WC} is average WC grain size.

In the case of the samples with the same amount of hard and binder phases, with the increase of WC grain size, the hardness of the cemented carbides decreases, but the difference between the two extremes of the hardness value is small. It is important to mention that less pronounced decrease of hardness is obvious for the cemented carbide composites with higher Ni content (i.e. 5, 7 and 9 wt.%). This is probably due to the change in

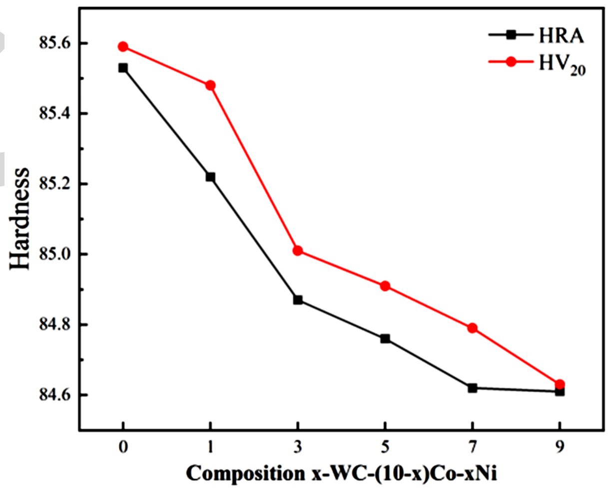

Figure 5. Rockwell and Vickers hardness of cemented carbides with different Co/Ni ratios

sintering process. Regrowth phenomenon is more active for lower Ni content and the effect of Ni on sintering reaches the saturation for higher Ni content. Saturated state will not lead to the additional WC grains growth, so the hardness reduction tends to be less pronounced.

3.3. Wear resistance

The wear resistance coefficient of the cemented carbides with different Co/Ni ratios, shown in Fig. 6, is directly proportional to the hardness and also shows a decreasing trend. However, the WC-5Co-5Ni specimen can be regarded as an inflexion point of its decrease, before which the wear resistance decreases more gently, and after which there is an obvious slippage. From the microscale analysis there is an obvious regrowth

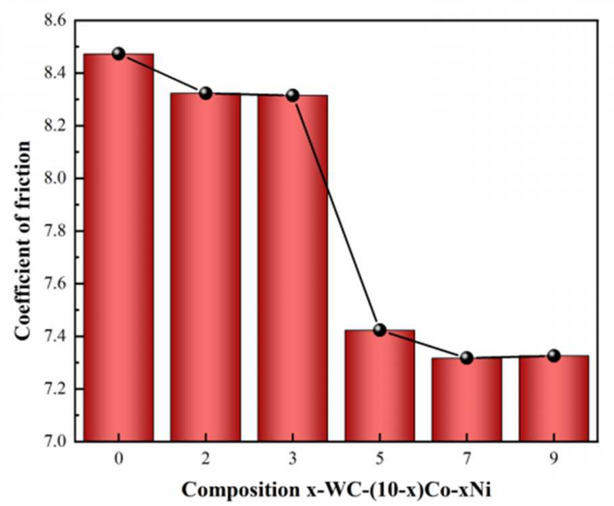

Figure 6. Friction coefficients of cemented carbides with different Co/Ni ratios

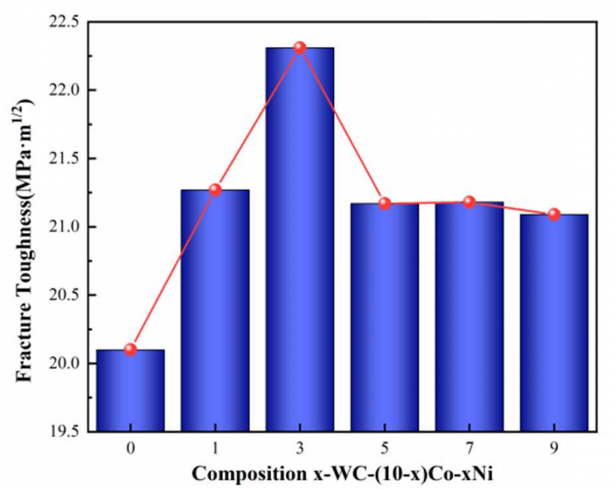

Figure 7. Fracture toughness of cemented carbides with different Co/Ni ratios

phenomenon and the emergence of larger areas of the bonded phase. It is well known that wear is mainly due to the deformation of the bonded phase, therefore the wear resistance will be drastically decreased in the composite with higher Ni content.

If we consider the crystal structure and mutual solubility, then the dense row hexagonal structure will be the ideal wear-resistant structure. Thus, since the structure of Co is particularly close to the dense row hexagonal structure, Co can improve the wear resistance coefficient of the composite. However, the higher solubility of WC in the bonding phase containing Ni than that with Co, additionally has influence on the wear resistance decreasing of the cemented carbides composites.

3.4. Fracture toughness

The fracture toughness of the composites was tested by the V-notch method, where P_{max} is the maximum critical pressure at which the sample will fracture and is substituted into Eq. 2 to calculate the fracture toughness (K_{IC}):

$$K_{IC} = \frac{P_{max}}{B\sqrt{W}} Y_C \tag{2}$$

where B is specimen width, W is specimen height and Y_C is dimensional coefficient (15.94).

As it can be seen from Fig. 7, the fracture toughness increases with the increase of Ni content and then decreases and stabilizes. The fracture toughness mainly reflects the degree of crack extension and the average grain size and the average free range are the main factors affecting the fracture toughness. Larger grains in the samples with higher Ni amount contribute to the increase of K_{IC}, but the bonding strength between the WC grains and the bonding phase is reduced with Ni addition which reduces the fracture toughness of cemented carbides. Thus, the observed highest fracture toughness of the WC-7Co-3Ni sample is a result of different effects together with the fact that an appropriate amount of Ni can stabilize the face-centred cubic Co phase at room temperature. Thus, the composite is strengthened to a certain extent which causes improvement of the fracture toughness for the composite with this Ni contents.

3.5. Flexural strength

Figure 8 shows the flexural strength of the WC-Co-Ni cemented carbides with different Co/Ni ratio. It can be seen that the bending strength of the cemented carbides decreases with the increase of Ni content, but there is not much difference between the bending strength of the WC-7Co-3Ni and WC-5Co-5Ni composites. Flexural strength indicates the comprehensive performance of cemented carbides, which is mainly related to factors such as WC grain size, Co binder phase content, organizational structure and porosity. Generally, the flexural strength of cemented carbides with various bonding phases decreases with the increase of grain size. This is mainly related to the fact that finer WC grains more easily disperse stress than coarse grains. Having larger grains in the specimen increases probability of

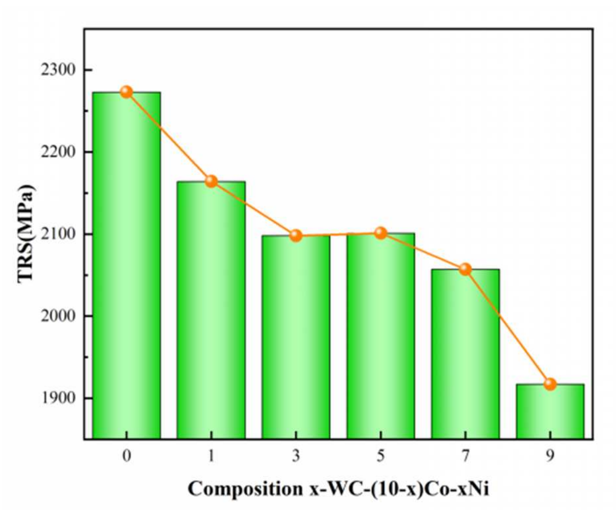

Figure 8. Flexural strength of cemented carbides with different Co/Ni ratios

forming a source of fracture under pressure. The addition of Ni promotes the grain coarsening and causes the decrease of the bending strength (Fig. 8). The difference in flexural strength between the WC-7Co-3Ni, WC-5Co-5Ni and WC-3Co-7 composites is small and obvious drop is observed for the WC-1Co-9Ni sample. The fracture of cemented carbides depends on the joint action of fracture source cracking and crack extension. Thus, this high drop can be explained with the increase of WC grain adjacency at high Ni content, which leads to the easier crack extension.

3.6. Corrosion resistance

Figure 9 shows the polarization curves of the WC-Co-Ni composites in a neutral solution of 3.5% NaCl. There is no big difference in the corrosion potential of the WC-10Co and WC-9Co-1Ni samples, but the corrosion current density decreases significantly, indicating that the addition of Ni has greatly improved the corrosion resistance of the composites in a neutral NaCl solution. With further increase of Ni content, the corrosion current density of the samples has only a slight increase (except for the WC-1Co-9Ni composite), indicating that Ni addition can effectively improve the corrosion resistance of the WC-Co-Ni composites. The corrosion potential of the WC-1Co-9Ni compared to the WC-10Co specimen is shifted positively by 0.18 V, and the corrosion current density decreased by one order of magnitude. This confirmed that replacing of Co with Ni in the cemented carbides binder phase can significantly improve the corrosion resistance of the composite in neutral solution.

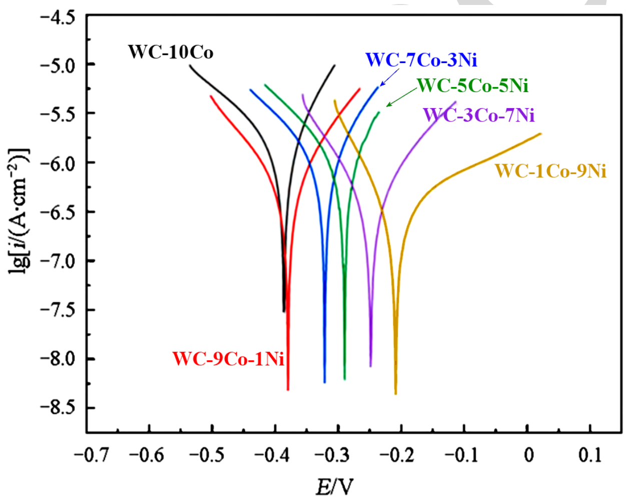

Figure 9. Polarization curves of cemented carbides with different Co/Ni ratios

IV. Conclusions

WC-Co-Ni cemented carbides with 90 wt.% WC and different Co/Ni mass ratios (10:0, 9:1, 7:3, 5:5, 3:7 and 1:10) were prepared by powder metallurgy method and sintering at 1450 °C under argon atmosphere. The purpose was to find an optimal Co/Ni ratio for reliable cutting tools and the following conclusions were obtained through a comprehensive analysis of various mechanical properties tests and corrosion experiments:

(1) The WC-10Co specimen has very uniform distribution of WC grains in the binder phase. With the increasing Ni content, the average WC grain size increases and the uniformity of size distribution decreases.
(2) The hardness, wear resistance coefficient and flexural strength of the WC-Co-Ni composites decrease continuously with the continuous increase of Ni content. On the other hand, the fracture toughness first increased and then decreased, with the maximal value of 22.32 MPa·m$^{1/2}$ for the sample WC-7Co-3Ni.
(3) Corrosion resistance of the WC-Co-Ni composites, analysed in aqueous solution with 3.5% NaCl, was gradually enhanced with the continuous increase of Ni content.
(4) The WC-7Co-3Ni sample has homogeneous microstructure with uniform WC grains, good comprehensive mechanical properties, microhardness of 84.86 HRA, wear resistance coefficient of 8.27, flexural strength of 2086 MPa, fracture toughness of 22.32 MPa·m$^{1/2}$, and good corrosion resistance with the current density of 1.37×10^{-6} A/cm^2. Compared with other composites, the WC-7Co-3Ni sample can better meet the performance requirements for shield tool with good corrosion and damage resistant, which is helpful to improve the service life of the tool.

Acknowledgement: This study was supported by the Science and Technology Enterprise Innovation Program of Shandong Province China (2023TSGC0961).

References

1.
2. L. Yang, X.J. Cao, Y. Wang, Y. Lian, Z. Guo, “Does metro expansion matter? Metro network enhances metro mode share of commuters living away from stations, but not those near stations”, *Travel Behaviour Soc.*, **34** (2024) 100664.
3. X. Meng, T. Ding, H. Wang, “Incentives for local government expenditures on people’s livelihood: the role of high-speed rail”, *Socio-Econom. Planning Sci.*, **89** (2023) 101700.
4. J. Song, A. Abuduwayiti, Z. Gou, “The role of subway network in urban spatial structure optimization – Wuhan city as an example”, *Tunn. Undergr. Spa. Tech.*, **131** (2023) 104842.
5. J. Xie, P. Li, M. Zhang, L. Cao, F. Jia, S. Li, “Analytical investigation of the shield-soil rotary friction on tunnelling-induced ground mechanical reactions”, *Comput. Geotechn.*, **165** (2024) 105922.
6. L. Yang, X. Guo, J. Chen, Y. Wang, H. Ma, Y. Li, Z. Yang, Y. Shi, “Vote-based feature selection method for stratigraphic recognition in tunnelling process of shield machine”, *Chin. J. Mech. Eng.*, **36** (2023) 128.

7. S. Kan, J. Chen, Y. Liang, Y. Wang, H. Zhou, "Research on lateral deformation control criteria of metro shield tunnels with excessive ellipticity", *Appl. Sci.*, **13** (2023) 12721.
8. Z. Li, Y. Li, J. Zhao, H. Li, B. Wang, "Reliability analysis of hinged hydraulic system of remanufactured EPB shield machine", *J. Phys. Conf. Ser.*, **2785** (2024) 012041.
9. Y. Zhang, G. Gong, H. Yang, J. Li, L. Jing, "From tunnel boring machine to tunnel boring robot: perspectives on intelligent shield machine and its smart operation", *J. Zhejiang Univer. Sci. A*, **25** (2024) 357–381.
10. J. Jin, Q. Jin, J. Chen, C. Wang, M. Li, L. Yu, "Prediction of the tunnelling advance speed of a super-large-diameter shield machine based on a KF-CNN-BiGRU hybrid neural network", *Measurement*, **230** (2024) 114517.
11. G. Chen, W. Li, F. Yang, T. Cao, Z. Wu, Y. Lu, C. Wu, "Study on resourceful treatment and carbon reduction intensity of metro shield slag: An example of a tunnel interval of Shenzhen Line 13", *Buildings*, **13** (2023) 2816.
12. X. Shen, X. Chen, X. Bao, R. Zhou, G. Zhang, "Real-time prediction of attitude and moving trajectory in shield tunneling based optimal input parameter combination using random forest deep learning method", *Acta Geotechnica*, **18** (2023) 6687–6707.
13. M. Yang, Y. Xia, Y. Ren, B. Zhang, Y. Wang, "Design of O-ring with skeleton seal of cutter changing robot storage tank gate for large diameter shield machine", *Tribology Int.*, **185** (2023) 108591.
14. B. Liu, M. Hu, B. Zhang, B. Li, B. Xu, C. Huang, H. Yu, J. Zhang, L. Gu, "Influence of abrasive waterjet pre-cutting slit on the performance of shield cutter cutting reinforced concrete", *Tunn. Undergr. Spa. Tech.*, **142** (2023) 105448.
15. X. Feng, Y. Wang, J. Han, Z. Li, L. Jiang, B. Yang, "Numerical simulation and experimental verification of the quenching process for Ti microalloying H13 steel used to shield machine cutter rings", *Metals*, **14** (2024) 313.
16. W. Yang, J. Zheng, R. Zhang, S. Liu, W. Zhang, "Dynamic prediction of over-excavation gap due to posture adjustment of shield machine in soft soil", *Underground Space*, **16** (2024) 44–58.
17. S. Zeng, Y. Jin, R. Zhou, X. Wu, W. Su, X. Tang, "Strengthening and toughening of WC-Ni alloys by adding novel (Ti,Hf,Ta,Nb,Zr)(C,N) high entropy powder", *Int. J. Refractory Met. Hard Mater.*, **118** (2024) 106436.
18. S. Xu, S. Wang, C. Xu, C. Zhao, W. Zhang, W. Wang, L. Chen, Q. Ren, Y. Pan, J. Li, G. Ren, F. Ni, J. Han, "Influence of starting WC particle size and sintering conditions on structure and properties of WC-Ni-Co coarse grain ceramics", *Process. Appl. Ceram.*, **18** (2024) 235–243.
19. S. Yang, D. Wang, Z. Xiao, "Study on surface properties of coated WC-Co alloy based on laser reduction process", *Ind. Lubr. Tribol.*, **76** (2024) 131–140.
20. M. Ostolaza, A. Zabala, J.I. Arrizubieta, I. Llavori, N. Otegi, A. Lamikiz, "High-temperature tribological performance of functionally graded Stellite 6/WC metal matrix composite coatings manufactured by laser-directed energy deposition", *Friction*, **12** (2023) 522–538.
21. Z. Zhao, R. Liu, J. Chen, X. Xiong, "Material extrusion printing of WC-8%Co cemented carbide based on partly water-soluble binder and post-processing", *J. Mater. Res. Technol.*, **29** (2024) 4394–4405.
22. R. Su, D. Hao, P. He, D. Wu, Q. Wang, H. Dong, H. Ma, "Effect of Co on creep and stress rupture properties of nickel-based superalloys - A review", *J. Alloys Compds.*, **967** (2023) 171744.
23. K.T. Suzuki, S. Omura, S. Tokita, Y.S. Sato, Y. Tatsumi, "Drastic improvement in dissimilar aluminum-to-steel joint strength by combining positive roles of silicon and nickel additions", *Mater. Design*, **225** (2023) 111444.
24. I.H. Lotfy, S.A. Mansour, A.M. El-Taher, "The dynamic and static mechanical characteristics of Sn-7Zn-based solder alloy modified with microalloying of In, Fe and Co elements", *J. Mater. Sci. Mater. Electron.*, **33** (2022) 26728–26743.
25. X. Wei, W. Zhu, A. Ban, D. Zhu, C. Zhang, H. Dong, "Effects of Co addition on microstructure and cavitation erosion resistance of plasma sprayed TiNi based coating", *Surf. Coat. Tech.*, **409** (2021) 126838.
26. Q. Liao, W. Wei, H. Zuo, X. Li, Z. Yang, S. Xiao, G. Wu, "Interfacial bonding enhancement and properties improvement of carbon/copper composites based on nickel doping", *Compos. Interf.*, **28** (2021) 637–649.